Simulation study of low emittance tuning of the Accelerator Test Facility damping ring at KEK

Kiyoshi Kubo

KEK, High Energy Accelerator Research Organization, 1-1, Oho, Tsukuba, Ibaraki 305-0801, Japan

(Received 25 June 2003; published 18 September 2003)

For damping rings of future linear colliders, extremely low vertical emittance will be required. In an electron circular accelerator, the dominant sources of the vertical emittance are the vertical dispersion in arc sections and the *x*-*y* orbit coupling, caused by various errors. A systematic method to correct the vertical dispersion and the orbit coupling based on beam position measurement has been developed. In this paper, simulation studies assuming realistic misalignments, performances of monitors, and correctors of the Accelerator Test Facility damping ring at KEK are presented.

DOI: 10.1103/PhysRevSTAB.6.092801 PACS numbers: 29.27.Fh, 29.20.Dh

I. INTRODUCTION

For damping rings of future linear colliders, extremely low vertical emittance will be required. In an electron circular accelerator, the dominant sources of the vertical emittance are the vertical dispersion in arc sections and the *x*-*y* orbit coupling, caused by various errors. We have developed a systematic method to correct the vertical dispersion and the orbit coupling based on beam position measurement. The method has been used for the ATF (Accelerator Test Facility) damping ring at KEK [1,2]. In this paper, simulations assuming realistic misalignment, performances of monitors, and correctors of the ATF damping ring are presented. The simulation results have shown that our method should work well. In recent operation of the ATF damping ring, the method has been applied typically every week and our target of the vertical emittance, less than 1% of the horizontal emittance, has been continuously achieved [3–5].

The computer code SAD [6] was used in the simulation for calculating closed orbit, dispersions, emittances, and various beam parameters for given conditions of the ATF damping ring.

II. ATF DAMPING RING

The ATF damping ring is designed to produce an extremely small vertical emittance beam as a test accelerator for future linear colliders. The shape of the ring is as a racetrack with two straight sections and two arc sections. Each arc is 41.7 m and each straight section is 27.6 m in length; circumference of the ring is 138.6 m. The lattice in the arc sections was designed as a focusing and defocusing (FODO) quadrupole using combined function bending magnets. There are 48 horizontal and 50 vertical steering magnets for the orbit correction. Beam positions are measured using 96 beam position monitors (BPM). Basically, every FODO cell has one horizontal steering magnet, one vertical steering magnet, and two BPM. There are 34 focusing and 34 defocusing sextupole magnets in the arc sections. For the purpose of coupling corrections, the trim windings of all 68 sextupole magnets have been arranged to produce skew quadrupole fields. There are no skew correctors in the dispersion free region.

III. MEASURES OF BEAM QUALITY

The dominant sources of the vertical emittance are the vertical dispersion in arc sections and the *x*-*y* orbit coupling. We introduce here two quantities, which characterize these sources of the vertical emittance, rms of the vertical dispersion in the arc sections, η_{arc} and the *x*-*y* orbit coupling, C_{xy}:

$$\eta_{\mathrm{arc}} \equiv \sqrt{\langle \eta_{y,\mathrm{BPM}}^2 \rangle_{\mathrm{arc}}}, \tag{1}$$

$$C_{xy} \equiv \sqrt{\frac{1}{N_{\mathrm{steers}}} \sum_{\mathrm{H\ steers}} \frac{\sum_{\mathrm{BPM}} \Delta y^2}{\sum_{\mathrm{BPM}} \Delta x^2}}, \tag{2}$$

where $\eta_{y,\mathrm{BPM}}$ is the vertical dispersion at a BPM which is evaluated from the difference of the beam position for different rf frequencies of the ring. The angle brackets denote the average over arc sections. C_{xy} is obtained from the beam positions while changing several horizontal steering magnets, one at a time. Here, Δx and Δy are horizontal and vertical beam position changes at each BPM in response to each horizontal steering magnet. N_{steers} is the number of used horizontal steering magnets. An average over several steering magnets is taken. It should be noted that both quantities can be obtained from measurement of the beam positions and monitoring the beam size is not necessary.

IV. SIMULATION PROCEDURE

In the simulation, misalignments of the magnets and errors of BPM were set. Then a sequence of the corrections, the rough closed orbit distortion (COD) correction, the COD correction, the vertical COD-dispersion correction, and the coupling correction were simulated. The

sequence is the same as the beam tuning in our actual beam operations.

A. Set misalignment of magnets and error of BPM

First, transverse offsets of all the magnets are set as actually measured and shown in Figs. 1 and 2. The vertical offset of each magnet was measured as a deviation from a reference plane. On the other hand, the horizontal offset was measured only as a deviation from the straight line connecting two nearby bending magnets. At this stage, the horizontal offsets of all the bending magnets were assumed to be zero. In order to consider the error of the measurement, random offsets were added for all magnets including the bending magnets. Random rotation errors of all the magnets were also set. In order to consider the misalignment of BPM and the calibration error of the electronics for BPM, each BPM was also assumed to have a random offset and rotation errors. For each BPM, the offset error was set with respect to the field center of the nearest magnet, which is a quadrupole magnet or a sextupole magnet. The random errors had Gaussian distribution and the errors of each magnet or each BPM were independent. As a standard condition, a set of rms of these errors was chosen as listed in Table I. Simulations with some different conditions were also performed. For each condition, 500 cases with different sets of errors from different random seeds were simulated.

Misalignment of the BPM was taken into account in the simulation as

$$x_{\mathrm{meas}} = (x - x_m - x_b)\cos\phi + (y - y_m - y_b)\sin\phi, \quad (3)$$

$$y_{\mathrm{meas}} = -(x - x_m - x_b)\sin\phi + (y - y_m - y_b)\cos\phi, \quad (4)$$

$$\eta_{y,\mathrm{meas}} = -\eta_x \sin\phi + \eta_y \cos\phi, \quad (5)$$

where x_{meas} and y_{meas} are the measured orbit positions at a BPM, x and y the real positions, x_m and y_m the offset error of the nearest magnet to the BPM, x_b and y_b the offset of the BPM with respect to the magnet, and ϕ the rotation

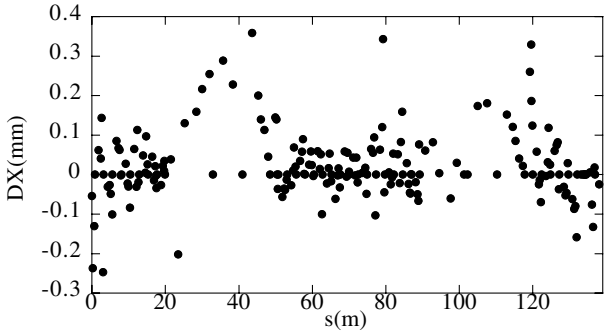

FIG. 1. Measured horizontal misalignment with respect to bending magnets.

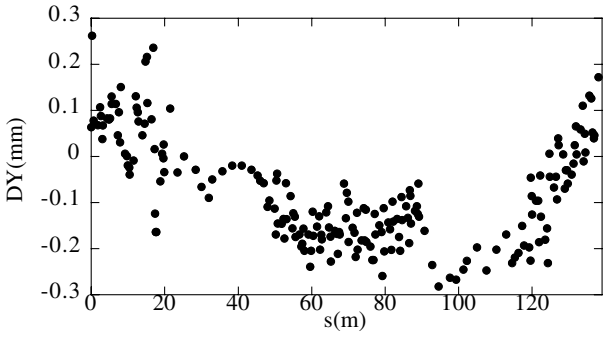

FIG. 2. Measured vertical misalignment.

error of the BPM. $\eta_{y,\mathrm{meas}}$ is the measured vertical dispersion at the BPM, η_x the real horizontal dispersion, and η_y the real vertical dispersion.

B. Rough COD correction

Because of the misalignment of the magnets, in most of the cases, COD was unreasonably large, and in some cases, the closed orbits cannot be found without any corrections. The purpose of this step is to make the closed orbit exist and reasonably small for the next step. All steering magnets were used to correct the orbits. In order to find the set of strengths of the steering magnets, we used a prepared routine in SAD, which is a step by step searching process to find a set of free parameters to satisfy required conditions. In our case, strength of all the steering magnets was set to be the free parameters and the conditions were chosen as

$$|x_{\mathrm{meas}}| < 2 \text{ mm} \quad \text{and} \quad |y_{\mathrm{meas}}| < 1 \text{ mm} \quad (6)$$

at all BPM. Only in very rare cases, SAD could not find the closed orbit with any set of magnet strengths probably because the misalignment of some magnets was too large. In those cases further steps were not performed and they were not included in the results. In some other cases the required conditions were not fully satisfied though the closed orbits were found. As long as there were closed orbits found, the results of this step were used as initial conditions of the next step.

C. COD correction

For the COD correction, responses of the horizontal and the vertical beam positions at every BPM to every

TABLE I. Errors in the standard condition.

Additional offset of magnet[a]	30 μm
Rotation of magnet	300 μrad
Offset of BPM[b]	300 μm
Rotation of BPM	20 mrad

[a]Added to measured misalignment.
[b]With respect to the nearest magnet.

steering magnet were calculated. SAD was used for this calculation assuming no misalignment of magnets and no skew fields. The set of responses is common for all simulated cases. We calculated responses to the unit change of kick angles of steering magnets as

$$R_x(i,\,p) = \frac{x_{i,p}(\theta)}{\theta}, \tag{7}$$

$$R_x(i,\,q) = \frac{y_{i,q}(\theta)}{\theta}, \tag{8}$$

where $x_{i,p}(\theta)$ is the horizontal closed orbit at the ith BPM as the result of a horizontal kick angle θ by the pth steering magnet, and $y_{i,q}(\theta)$ the vertical closed orbit at the ith BPM as the result of a vertical kick angle θ by the qth steering magnet. Though the orbit change is not linear for large kick angles, θ, these responses are approximately constant for small angles. Here, θ was chosen to be 0.1 mrad, which was small enough for the linear approximation.

The horizontal and vertical closed orbits were corrected using all the horizontal and vertical steering magnets, respectively. This correction minimizes

$$\langle x^2_{\rm meas}\rangle \equiv \frac{1}{N_{\rm BPM}}\sum_i x^2_{i,\rm meas} \tag{9}$$

and

$$\langle y^2_{\rm meas}\rangle \equiv \frac{1}{N_{\rm BPM}}\sum_i y^2_{i,\rm meas}, \tag{10}$$

where $x_{i,\rm meas}$ and $y_{i,\rm meas}$ are the measured horizontal and vertical orbit positions at the ith BPM and $N_{\rm BPM}$ is the number of BPM. The sets of additional kick angles θ_p and θ_q were calculated to minimize

$$\sum_i \left[x_{i,\rm meas} - \sum_p R_x(i,\,p)\theta_p \right]^2 \tag{11}$$

and

$$\sum_i \left[y_{i,\rm meas} - \sum_q R_y(i,\,q)\theta_q \right]^2. \tag{12}$$

Similar to the COD correction, an iteration was done. The kick angles were changed by 0.7 times the calculated θ_q in the first step and by full of θ_q in the second step.

E. Coupling correction

The coupling correction is to minimize the x-y orbit coupling by using a suitable combination of the skew quadrupole fields in the ring. This correction minimizes

$$\sum_i \left[y_{i,\rm meas} - \sum_q R_y(i,\,q)\theta_q \right]^2 + r^2 \sum_i \left[\eta_{y,i,\rm meas} - \sum_q R_{Dy}(i,\,q)\theta_q \right]^2. \tag{16}$$

$$C_{xy,\rm meas} \equiv \sqrt{\frac{1}{N_{\rm steer}}\sum_{\rm steer}\frac{\sum \Delta y^2_{\rm meas}}{\sum \Delta x^2_{\rm meas}}} \tag{17}$$

using skew quadrupole correctors. $N_{\rm steer}$ is the number of the used steering magnets, $\Delta x_{\rm meas}$ is the measured horizontal orbit change, and $\Delta y_{\rm meas}$ is the measured vertical orbit change due to the change of each steering magnet.

Because of the rotation errors of magnets, the rotation error of BPM, and the nonlinear fields of the sextupole magnets the real responses are different from $R_x(i,\,p)$ and $R_y(i,\,q)$ which were calculated without errors. To make the correction better, an iteration was done. The kick angle of each steering magnet was changed by 0.7 of the calculated value from Eq. (11) in the first step. Then the closed orbit was simulated again, and the new set of additional kick angles is calculated. The second time, the kick angles were changed as calculated from Eq. (11).

D. Vertical COD-dispersion correction

Similar to the COD correction, the response of the vertical dispersion at every BPM to every steering magnet was calculated. SAD was used for this calculation assuming no misalignment of magnets and no skew fields. The set of responses is common for all simulated cases. We calculated responses to the unit change of kick angles of steering magnets as

$$R_{Dy}(i,\,q) = \frac{\eta_{y,i,q}(\theta)}{\theta}, \tag{13}$$

where $\eta_{y,i,q}(\theta)$ is the vertical dispersion at the ith BPM as the result of the vertical kick angle θ by the qth steering magnet.

The vertical dispersion was corrected keeping the vertical closed orbit small, using all the vertical steering magnets. Similar techniques of simultaneous orbit-dispersion correction are found in previous works as Refs. [7,8].

This correction minimizes

$$\langle y^2_{\rm meas}\rangle + r^2\langle \eta^2_y\rangle, \tag{14}$$

where

$$\langle \eta^2_{y,\rm meas}\rangle \equiv \frac{1}{N_{\rm BPM}}\sum_i \eta^2_{y,i,\rm meas}, \tag{15}$$

$\eta_{y,i,\rm meas}$ is the measured vertical dispersion at the ith BPM. The constant factor r decides the relative weight of the beam positions and dispersions in this correction.

The set of additional kick angles θ_q was calculated to minimize

Two horizontal steering magnets, which are apart by approximately $3/2\pi$ in horizontal and $1/2\pi$ in vertical phase advance, were chosen to evaluate the quantity. There are two families of the sextupole magnets, each of which consists of 34 magnets. All magnets of one family, 34 skew correctors, were used in this simulation. Responses of the vertical closed orbit at all BPM to each of the two steering magnets were calculated with a certain strength of every skew corrector, one by one. This calculation assumed no misalignment of magnets; the set of the responses is common for all simulated cases. Then, we calculated responses to the unit strength of each skew quadrupole and each corrector as

$$S_{i,p,j} = \frac{y_{i,p,j}(\theta, k)}{\theta k}, \tag{18}$$

where $y_{i,p,j}(\theta, k)$ is the vertical closed orbit at ith BPM as the result of the horizontal kick angle θ by the pth steering magnet with the strength of the jth skew corrector k. Note that

$$y_{i,p,j}(\theta, k) = 0 \qquad (\theta = 0 \quad \text{or} \quad k = 0), \tag{19}$$

because the calculation was done without any errors.

The set of skew quadrupole strengths for the correction was calculated to minimize

$$\sum_p \frac{\sum_i (y_{i,p,\mathrm{meas}}(\theta_p) - y_{i,p,\mathrm{meas}}(0) - \delta y_{i,p})^2}{\sum_i [x_{i,p,\mathrm{meas}}(\theta_p) - x_{i,p,\mathrm{meas}}(\theta_p)]^2}, \tag{20}$$

where p is the index for the used horizontal steering magnets, and i the index for BPM. $x_{i,p,\mathrm{meas}}(\theta)$ and $y_{i,p,\mathrm{meas}}(\theta)$ are the measured horizontal and vertical positions at ith BPM with the kick angle θ of the pth horizontal steering magnet. $\delta y_{i,p}$ are the expected changes of the vertical position response to the steering magnet due to a set of skew quadrupole fields, which is expressed as

$$\delta y_{i,p} = \sum_j S_{i,p,j} \theta_p k_j. \tag{21}$$

F. Calculation of beam quality

After each correction, the transverse emittances of the normal modes were calculated using the SAD program [9]. Because of residual coupling between the degrees of freedom of the transverse motion, these normal modes are not exactly in the physical horizontal and vertical planes. If the coupling is not very large, each of the normal modes can be considered as a horizontal-like or a vertical-like mode. In this paper, let us call the emittance of the vertical-like normal mode simply as "vertical emittance" and write ϵ_y.

In experimental measurements, the apparent vertical emittance is evaluated as

$$\epsilon_{y,\mathrm{ap}} = \sigma_y^2 / \beta_y, \tag{22}$$

where σ_y is the measured beam size and β_y the beta function at beam size monitors in the ring. There are two beam size monitors in the ATF ring, a synchrotron radiation (SR) monitor [10] and a laser wire (LW) monitor [11].

In addition, emittance of the beam is also measured after extraction from the ring [12]. If coupling components are absent in the extraction line, the projected vertical emittance ($\epsilon_{y,\mathrm{pr}}$) is evaluated from beam sizes at four or more positions in the beam line. $\epsilon_{y,\mathrm{pr}}$ is constant in the beam line.

For comparison with actual measurements, $\epsilon_{y,\mathrm{ap}}$ at the SR monitor and at the LW monitor and $\epsilon_{y,\mathrm{pr}}$ at the extraction were also calculated using the SAD program.

In the calculation of the emittance, only single particle dynamics was considered and the effects of intrabeam scattering were not included though they can be significant in actual applications.

V. RESULTS OF SIMULATIONS

A. Results with standard parameters

First, let us show how the corrections are effective for making a low emittance beam. The vertical emittance, ϵ_y, rms of the vertical dispersion in the arc sections, η_{arc}, and the x-y orbit coupling, C_{xy}, were calculated after each of the correction. The calculated horizontal emittance in the ATF damping ring without intrabeam scattering is 1.1×10^{-9} rad m and it is not sensitive to the errors and corrections considered here.

Figure 3 shows the distribution of ϵ_y after (a) COD correction, (b) COD-dispersion correction, and (c) coupling correction, respectively. Figure 4 shows the distribution of η_{arc} and Fig. 5 shows the distribution of C_{xy} after the three correction stages.

The vertical emittance, ϵ_y, is significantly reduced in both the COD-dispersion correction and the coupling correction. The averages of ϵ_y and the ratio of the random seeds which gave smaller ϵ_y than our target 1.1×10^{-11} rad m, at each correction stage, are summarized in Table II.

The COD-dispersion correction makes C_{xy} slightly larger and the coupling correction makes η_{arc} slightly larger. In principle, it is better to correct COD, dispersion, and coupling simultaneously. But in practice, it is easier to perform separately the COD-dispersion correction and the coupling correction. The simulation showed this practical method works well.

Figure 6 shows ϵ_y as a function of η_{arc} and Fig. 7 shows ϵ_y as a function of C_{xy} after (a) COD correction, (b) COD-dispersion correction, and (c) coupling correction, respectively. Each point corresponds to one random seed for the misalignments and BPM errors. It is shown that the vertical dispersion is the dominant source of the vertical emittance after the COD correction. Then, the orbit coupling is the dominant source after the

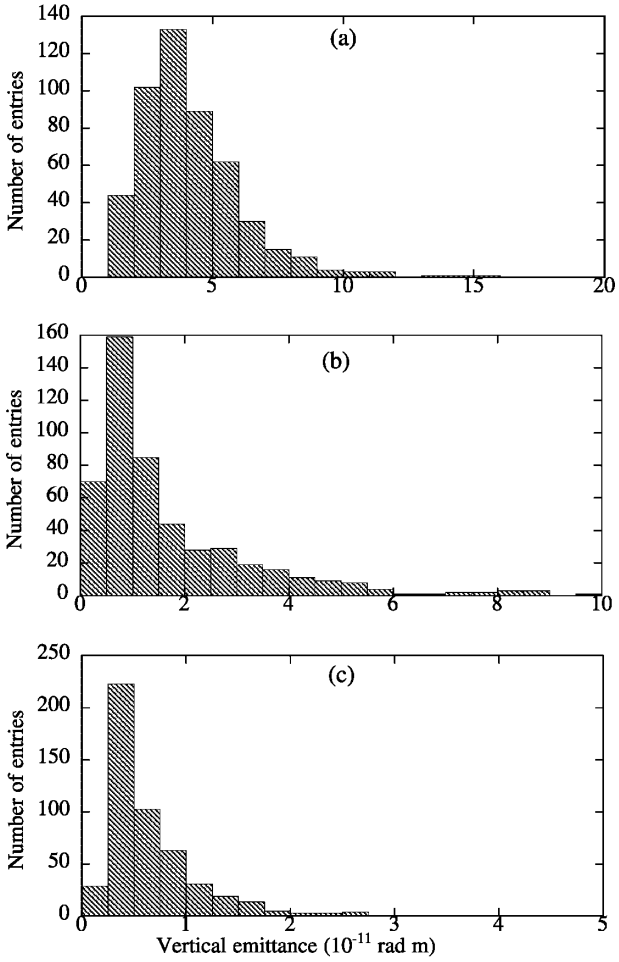

FIG. 3. Distribution of ϵ_y (10^{-11} rad m) (a) after COD correction, (b) after COD-dispersion correction, and (c) after coupling correction. Note the different horizontal scales.

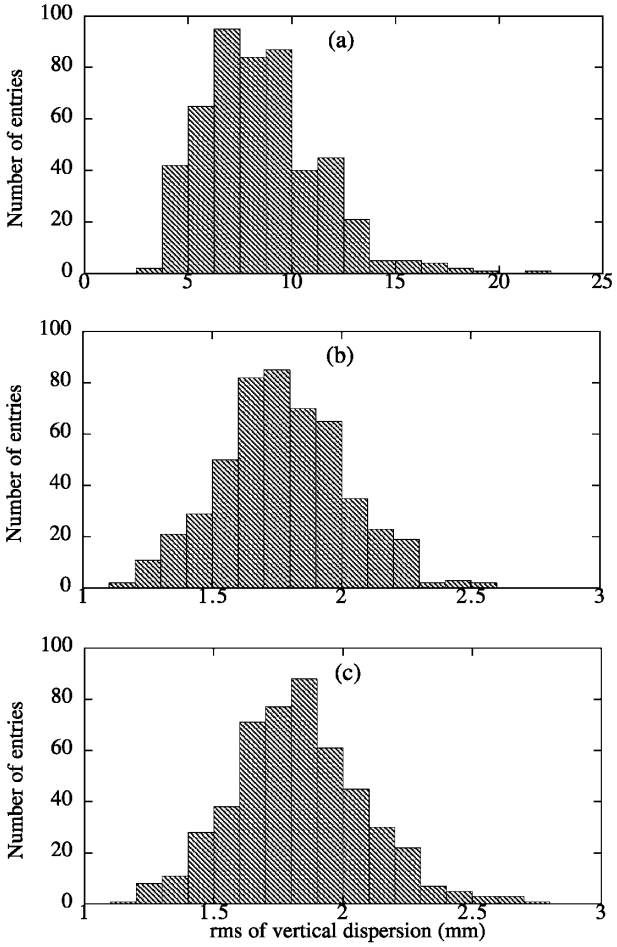

FIG. 4. Distribution of η_{arc} (mm) (a) after COD correction, (b) after COD-dispersion correction, and (c) after coupling correction. Note the different horizontal scales.

COD-dispersion correction, suggesting that our sequence of the corrections is appropriate.

B. Choice of factor r

The factor r in Eq. (14) should be chosen as the ratio of the expected error of the vertical dispersion and the expected error of the beam position. The expected vertical position error is the same as the expected BPM offset error, assuming the rotation error is not very large. On the other hand, the expected vertical dispersion error will be dominantly from the BPM rotation error and expressed as

$$\sigma_{\eta_y} \approx \sigma_{\eta_x}\sigma_\theta, \tag{23}$$

where σ_θ is the rms of the rotation error of BPM. σ_{η_x} is the rms of the horizontal dispersion, which is about 0.1 m in the ATF damping ring. And the factor r should be chosen as

$$r \approx \frac{\sigma_a}{\sigma_{\eta_y}} \approx \frac{\sigma_a}{\sigma_{\eta_x}\sigma_\theta}, \tag{24}$$

where σ_a is the rms of the offset error of BPM.

Simulation was performed for several choices of the factor r and the different BPM rotation and offset errors. Figure 8 shows expected ϵ_y as a function of r for different BPM rotation errors, $\sigma_\theta = 0$, 0.02, 0.05, and 0.1 rad, after the coupling correction where σ_a was set to be 0.3 mm. Each point in the figure indicates the average from 500 random seeds. Figure 9 shows expected ϵ_y as a function of r for different BPM offset errors, σ_a from 0 to 0.5 mm, after the coupling correction, where σ_θ was set to be 0.02 rad.

TABLE II. Simulated vertical emittance after each consecutive correction.

Correction	Average (rad m)	Ratio of $<1.1 \times 10^{-11}$ rad m
COD	2.28×10^{-11}	20%
COD dispersion	1.67×10^{-11}	51%
Coupling	0.58×10^{-11}	91%

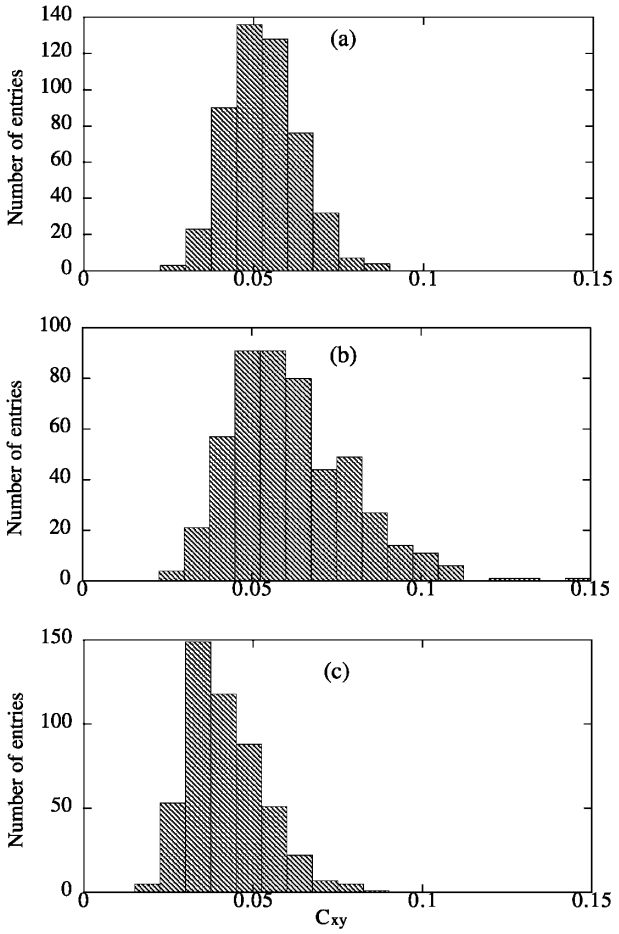

FIG. 5. Distribution of C_{xy} (a) after COD correction, (b) after COD-dispersion correction, and (c) after coupling correction.

Except for the case $\sigma_\theta = 0.1$, ϵ_y does not strongly depend on r if $r \geq 0.02$. In the case $\sigma_\theta = 0.1$, it increases with r in the region $r \geq 0.02$.

In conclusion, the expected vertical emittance is minimal around $r = 0.05$ and not a strong function of the factor r if $\sigma_\theta \leq 0.05$. Because $\sigma_\theta \leq 0.05$ is a reasonable assumption, we set r to be 0.05 as a standard.

C. Effects of BPM errors

Unknown misalignment and any imperfection of the calibration of the BPM system will cause systematic errors of the measured beam positions. This error was simulated as a random offset and a random rotation around the beam axis of each BPM. The measured dispersion, which is calculated from the difference of the beam positions with different beam energies, is not affected by the offset error. Also the measured coupling, which is calculated from the difference of the beam positions with different setting of the magnets, is not affected by the offset error either. On the other hand, the rotation error causes errors in the dispersion and the coupling, in which small vertical position differences

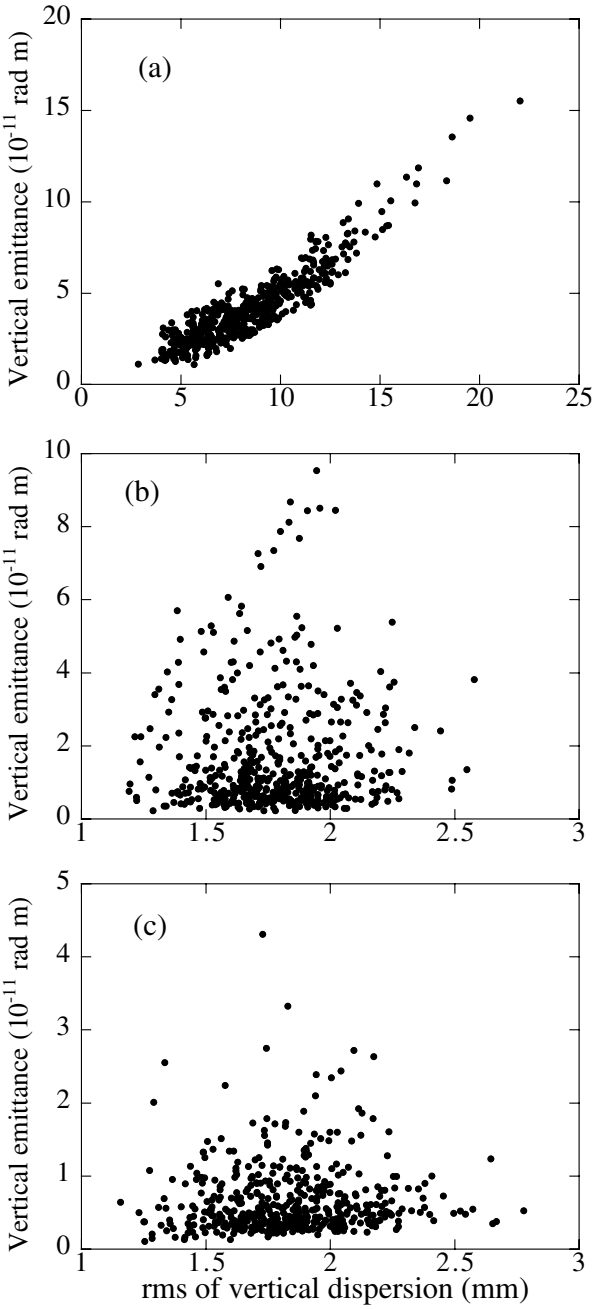

FIG. 6. ϵ_y vs η_{arc} (a) after COD correction, (b) after COD-dispersion correction, and (c) after coupling correction.

should be measured with large horizontal position differences.

In the ATF damping ring, for dispersion measurement, orbits are measured with momentum offsets of about 1.0%. The changes of the horizontal orbit at BPM in the arc sections are typically 1 mm, where the horizontal dispersion is about 0.1 m. Since the vertical dispersion should be within roughly 5 mm for small emittance (see Fig. 6), the vertical orbit change should be measured with an accuracy of 50 μm or better. In orbit coupling measurements, the horizontal orbit is also changed typically

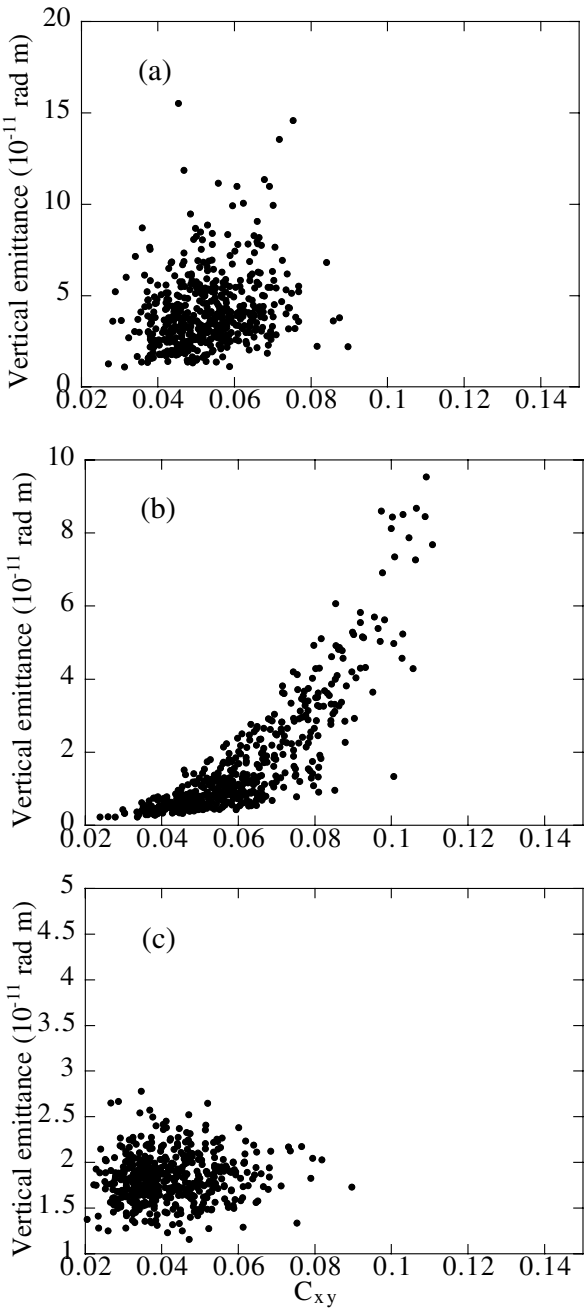

FIG. 7. ϵ_y vs C_{xy} (a) after COD correction, (b) after COD-dispersion correction, and (c) after coupling correction.

by about 1 mm and the accuracy for the vertical position difference should be better than about 50 μm, because C_{xy} should be, roughly speaking, less than 0.05 (see Fig. 7). Though the resolution of our BPM system is much better than the required accuracy the calibration error of the system may be significant.

Here, effects of the BPM errors after all corrections are discussed based on simulations.

The top graph of Fig. 10 shows the vertical emittance as a function of the BPM offset error, σ_a with $\sigma_\theta = 0.02$ rad and $r = 0.05$. The bottom graph of Fig. 10 shows the

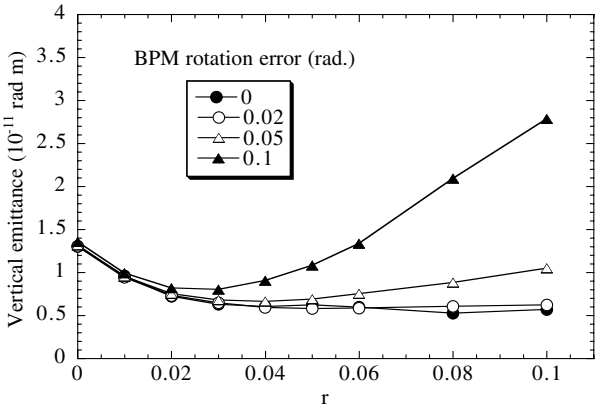

FIG. 8. ϵ_y vs r after coupling correction for different BPM rotation errors. BPM offset error was set as 0.3 mm.

vertical emittance as a function of the BPM rotation error, σ_θ, with $\sigma_a = 0.3$ mm and $r = 0.005$. Each point represents the average from 500 random seeds for the errors and the error bar shows the standard deviation.

As shown in Fig. 10, the expected vertical emittance after corrections is strongly correlated with the offset error of BPM. On the other hand, it is not sensitive to the BPM rotation error.

Averages of the real vertical dispersion, $\eta_{\rm arc}$, the apparent dispersion, $\eta_{\rm arc,meas}$, the real coupling, C_{xy}, and the apparent coupling, $C_{xy\rm meas}$ over 500 random seeds are shown in Fig. 11 as functions of the BPM offset error, σ_a, in the case $\sigma_\theta = 0.02$ rad and $r = 0.05$. $\eta_{\rm arc,meas}$ is defined as

$$\eta_{\rm arc,meas} \equiv \sqrt{\langle \eta^2_{y,\rm BPM,meas}\rangle_{\rm arc}}, \tag{25}$$

where $\eta_{y,\rm BPM,meas}$ is the measured vertical dispersion at a BPM and the angle brackets denote the average over arc sections. The real and apparent vertical dispersions are weakly dependent on σ_a and the real and apparent

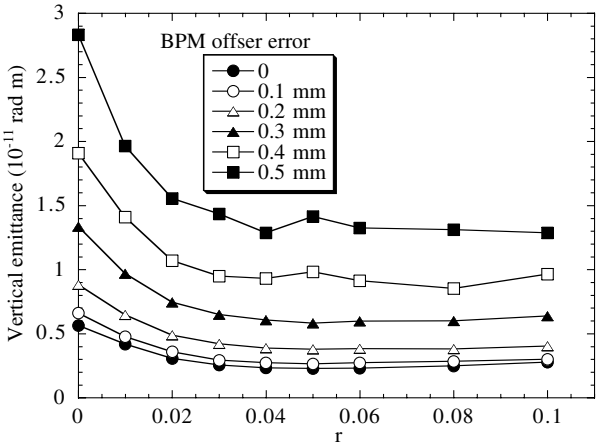

FIG. 9. ϵ_y vs r after coupling correction for different BPM offset errors. BPM rotation error was set as 0.02 rad.

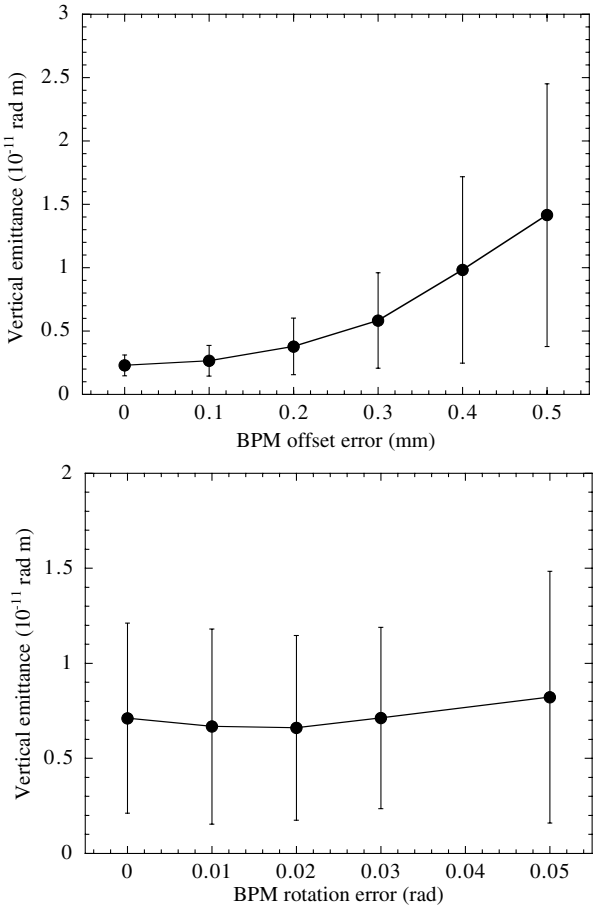

FIG. 10. Averages of ϵ_y vs (top panel) BPM offset error (σ_a) and (bottom panel) BPM rotation error (σ_θ) after the coupling correction. Error bars indicate the standard deviations.

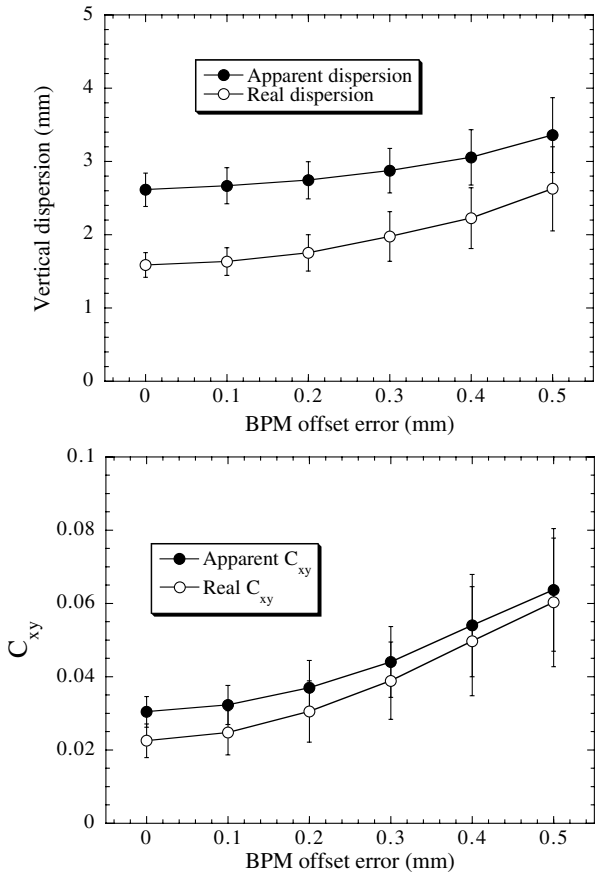

FIG. 11. Averages of (top panel) $\eta_{\mathrm{arc,meas}}$ and η_{arc}, (bottom panel) $C_{xy\mathrm{meas}}$ and C_{xy} vs σ_a after the coupling correction. The error bars indicate the standard deviations.

couplings are strongly dependent on σ_a. These dependences suggest that to reduce the BPM offset error is important to reduce the emittance sources, especially the orbit coupling.

Averages of η_{arc}, $\eta_{\mathrm{arc,meas}}$, C_{xy}, and $C_{xy\mathrm{meas}}$ over 500 random seeds are shown in Fig. 12 as functions of the BPM rotation error, σ_θ, in the case $\sigma_a = 0.3$ mm and $r = 0.05$. The apparent vertical dispersion and coupling are strongly dependent on σ_θ though the real vertical dispersion and coupling are not very sensitive to σ_θ. The corrections will not be significantly affected by the BPM rotation error. The real vertical dispersion and the real orbit coupling should have patterns defined by the optics. The random rotation error will hardly produce such patterns. Then the random error will be smeared out and will not affect the corrections though the apparent dispersion and coupling will be increased. In conclusion, the BPM rotation error is not as important as the offset error in the simulated region.

In Fig. 13 rms of horizontal and vertical COD are shown as functions of the BPM offset error, σ_a, in the case $\sigma_\theta = 0.02$ rad and $r = 0.05$. rms of the real and apparent COD are not significantly different and they are similar to the BPM offset error in the cases of large error. The result shows that the amount of BPM offset error can be roughly estimated from measured COD.

D. Apparent emittance

It should be noted that the vertical emittance shown in previous sections is different from what is usually measured, as mentioned in Sec. IIII F.

Here, we compare the simulated normal mode emittance, ϵ_y, and simulated "measured" emittances, apparent emittance at a SR monitor, at a LW monitor, and projected emittance at the extraction point.

Fig. 14, shows simulated $\epsilon_{y,\mathrm{ap}}$ at the LW monitor as a function of the normal mode emittance, ϵ_y. Figure 15 shows $\epsilon_{y,\mathrm{ap}}$ at the SR monitor and Fig. 16 $\epsilon_{y,\mathrm{pr}}$ as a function of ϵ_y. Each figure shows the results from 500 random seeds in the case of $\sigma_a = 0.3$ mm, $\sigma_\theta = 0.02$, and $r = 0.05$. Correlation between $\epsilon_{y,\mathrm{ap}}$ at the LW monitor and that at the SR monitor is also shown in Fig. 17.

Figures 14–16, indicate that the apparent (measured) vertical emittances are significantly larger than the normal mode emittance, typically by a factor of 1.5. Figure 17

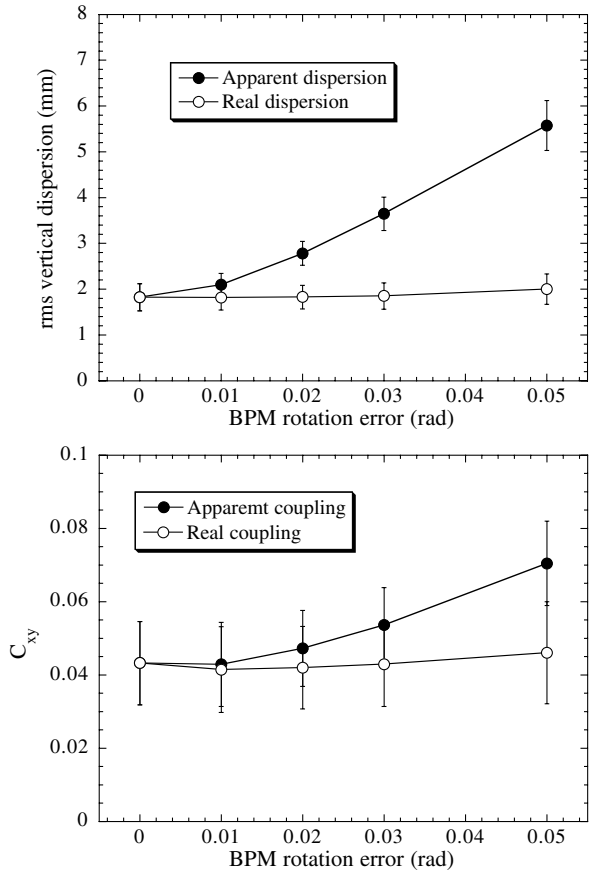

FIG. 12. Averages of (top panel) $\eta_{\mathrm{arc,meas}}$ and η_{arc}, (bottom panel) $C_{xy\mathrm{meas}}$ and C_{xy} vs σ_θ after the coupling correction. The error bars indicate the standard deviations.

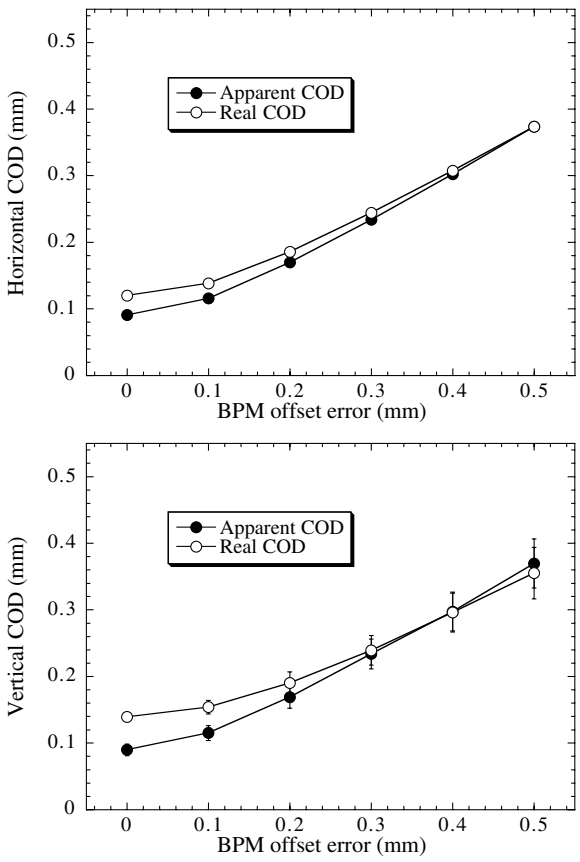

FIG. 13. Averages of rms of the (top panel) horizontal and (bottom panel) vertical COD vs σ_a after the coupling correction. The error bars indicate the standard deviations.

shows apparent emittances measured at different monitors that can also be significantly different from each other, depending on the condition of the errors and corrections. These facts should be considered when the simulation is compared with experimental data.

The normal mode emittance can be evaluated from the accurate measurement of horizontal, vertical, and slant beam sizes at four or more positions in the beam line. Using such data, and using four or more skew quadrupole magnets, it is possible to correct the x-y coupling and make the projected vertical emittance as small as the normal mode emittance [13]. For our purpose, using small emittance beams for linear colliders, this coupling correction, after extraction, will be desirable.

VI. CONCLUSIONS

Simulations of low emittance tuning in the ATF damping ring, assuming realistic errors, are presented. There are two primary sources of the vertical emittance, the vertical dispersion and the x-y orbit coupling. In the tuning method, the vertical dispersion is corrected using the vertical steering magnets first. Then the x-y coupling

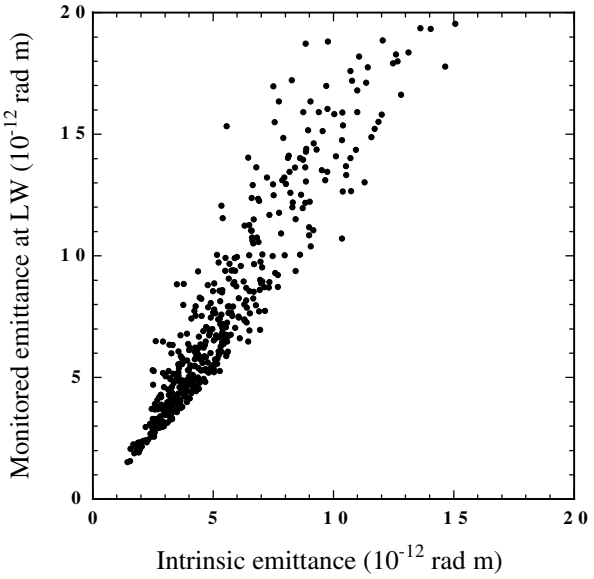

FIG. 14. $\epsilon_{y,\mathrm{mon}}$ at the LW monitor vs the intrinsic emittance, ϵ_y.

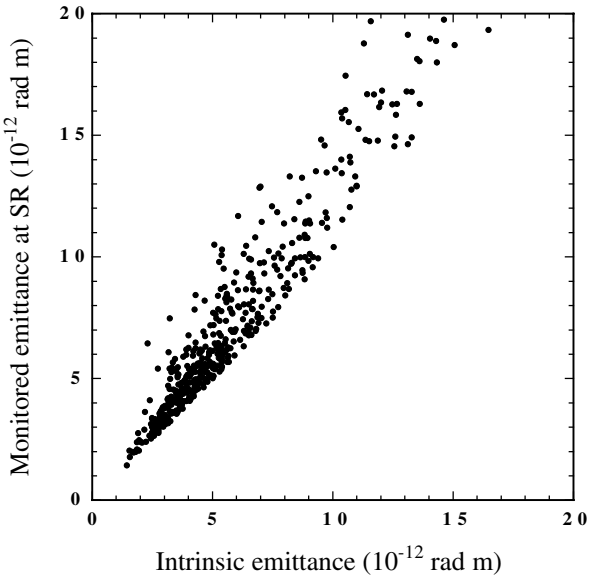

FIG. 15. $\epsilon_{y,\mathrm{mon}}$ at the SR monitor vs ϵ_y.

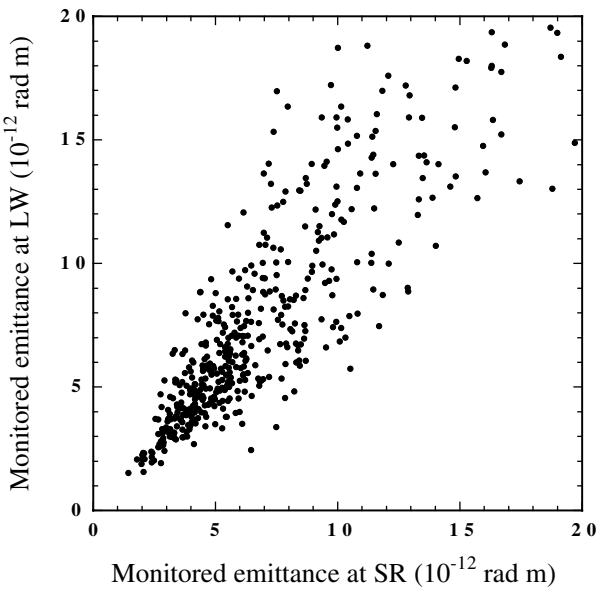

FIG. 17. $\epsilon_{y,\mathrm{mon}}$ at the LW monitor vs $\epsilon_{y,\mathrm{mon}}$ at the SR monitor.

is corrected using the skew quadrupole correctors. These corrections are based only on the measured closed orbit.

The simulation results have shown that our method should work well for making vertical emittance smaller than our target, 1% of the horizontal emittance.

For even lower vertical emittance, it is essential to reduce the offset error of BPM with respect to magnet field centers. On the other hand, the rotation error of BPM will not be so important for the vertical emittance though the apparent vertical dispersion and the apparent coupling will be strongly affected.

We roughly estimated the offset error of BPM at about 0.3 mm. Using a beam based technique [14], it will be possible to reduce the offset error less than 0.1 mm without any mechanical realignments. Referring to Fig. 10, the expected vertical emittance will be as small as 3×10^{-12} rad m.

It should be noted that the apparent vertical emittance or vertically projected emittance tends to be significantly larger than the normal mode emittance due to residual x-y coupling.

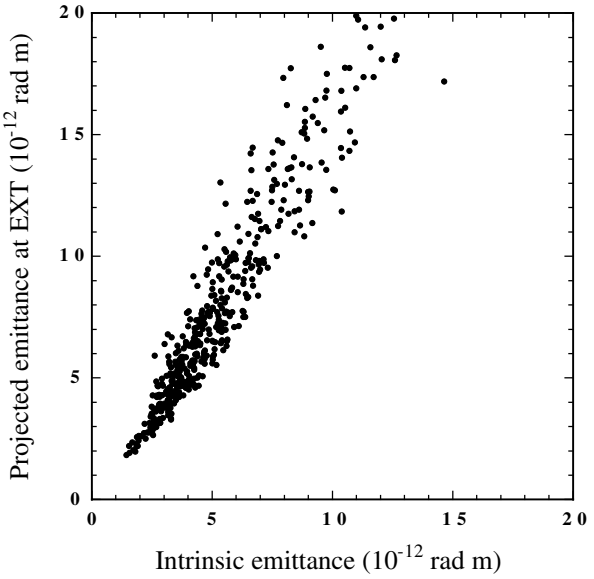

FIG. 16. $\epsilon_{y,\mathrm{proj}}$ vs ϵ_y.

ACKNOWLEDGMENTS

This work is closely related to the beam operation of the ATF (Accelerator Test Facility) at KEK. The author would like to thank all members of the ATF Collaboration, especially J. Urakawa and H. Hayano (KEK) for leading this project, T. Raubenheimer, M. Ross, M. Woodley (SLAC), A. Wolski (LBL), and N. Toge (KEK) for useful discussions and suggestions. I also thank K. Oide (KEK) for answering various questions on the SAD program.

[1] KEK internal Report No. 2000-6, 2000, edited by H. Hayano, K. Kubo, M. Ross, N. Toge, J. Urakawa, and F. Zimmermann.

[2] K. Kubo, H. Hayano, S. Kamada, M. Kuriki, S. Kuroda, T. Naito, T. Okugi, N. Terunuma, N. Toge, J. Urakawa, and M. Takano, in *Proceedings of the Seventh European Particle Accelerator Conference, Vienna, 2000* (Austrian Academy of Sciences Press, Vienna, 2000), pp. 483–485.

[3] ATF Collaboration, K. Kubo, Phys. Rev. Lett. **88**, 194801 (2002).

[4] H. Sakai, Y. Honda, N. Sasao, S. Araki, H. Hayano, Y. Higashi, K. Kubo, T. Okugi, T. Taniguchi,

N. Terunuma, J. Urakawa, and M. Takano, Phys. Rev. ST Accel. Beams **5**, 122801 (2002).

[5] ATF Collaboration, Y. Honda (to be published).

[6] SAD is a computer program for accelerator design, http://acc-physics.kek.jp/SAD/sad.html

[7] T. O. Raubenheimer and R. D. Ruth, Nucl. Instrum. Methods Phys. Res., Sect. A **302**, 191 (1991).

[8] R. Assmann, P. Raimondi, G. Roy, and J. Wenninger, in *Proceedings of the Seventh European Particle Accelerator Conference, Vienna, 2000* (Ref. [2]), pp. 1462–1464.

[9] K. Ohmi, K. Hirata, and K. Oide, Phys. Rev. E **49**, 751 (1994).

[10] T. Naito, H. Hayano, K. Kubo, T. Mitsuhashi, N. Terunuma, N. Toge, J. Urakawa, T. Okugi, and S. Kashiwagi, in *Proceedings of the Particle Accelerator Conference, New York, 1999* (IEEE, Piscataway, NJ, 1999), pp. 492–494.

[11] H. Sakai, N. Sasao, S. Araki, Y. Higashi, T. Okugi, T. Taniguchi, J. Urakawa, and M. Takano, Nucl. Instrum. Methods Phys. Res., Sect. A **455**, 113 (2000).

[12] H. Hayano, in *Proceedings of the XX International Linac Conference, Monterey, 2000* (SLAC, Stanford, 2000), pp. 146–148.

[13] M. Woodley and P. Emma, in *Proceedings of the XX International Linac Conference, Monterey, 2000* (Ref. [12]), pp. 196–198.

[14] M. Ross, J. Nelson, M. Woodley, and A. Wolski, in *Proceedings of the Eighth European Particle Accelerator Conference, Paris, 2002* (EPS-IGA/CERN, Geneva, 2002), pp. 431–433.